STM JOURNALS

Journal of
Polymer & Composites

https://journals.stmjournals.com/jopc

ISSN: 2321-2810 (Online)
ISSN: 2321-8525 (Print)
Volume 14, Issue 5, 2026
September–October
DOI (Journal): 10.37591/JoPC

Research JoPC

Studies on the Self-Assembly of Steroids and DNA Mediated by Naphthalene-Based Amphiphilic Block Copolymer

S. Prakash[1], N. Haridharan[2,*]

Abstract

Amphiphilic block copolymers have attracted considerable interest in pharmaceutical and biomedical applications, including controlled drug release, gene delivery, and biomolecular sensing. In this study, fluorescent amphiphilic block copolymers were designed to facilitate interactions with biological molecules, such as DNA and antiviral agents, enabling their behavior to be monitored through fluorescence spectroscopy. Two novel block copolymers, poly(methyl methacrylate)-b-poly(dimethylaminoethyl methacrylate-co-naphthyl methacrylate) [PMMA-b-P(DMAEMA-co-NMA)] and poly(styrene)-b-poly(tert-butyl acrylate-co-naphthyl methacrylate) [PS-b-P(t-BA-co-NMA)], were synthesized successfully via atom transfer radical polymerization (ATRP) using Copper(I) Bromide (CuBr) as catalyst and N,N,N',N'',N''-pentamethyldiethylenetriamine (PMDETA) as ligand. To establish steroid functionality into the polymer architecture, a steroid-based initiator has been prepared by reacting ergosterol with 2-bromoisobutyryl bromide. Gel permeation chromatography (GPC), proton nuclear magnetic resonance (^{1}H NMR), Fourier-transform infrared (FTIR), and UV–Visible spectroscopy was utilized to characterize the synthesized polymers. The monomer conversion and the increasing in molecular weight were revealed by polymerization kinetics which indicated controlled polymer growth. The fluorescence characteristics of the block copolymers were investigated, and their self-assembly into micellar structures in aqueous media was confirmed. Furthermore, DNA-binding studies demonstrated that the steroid-containing block copolymers exhibited progressive fluorescence quenching with increasing DNA concentration (1–10 µg), suggesting effective polymer–DNA interactions and supporting the formation of self-assembled nanostructures.

Graphical Abstract

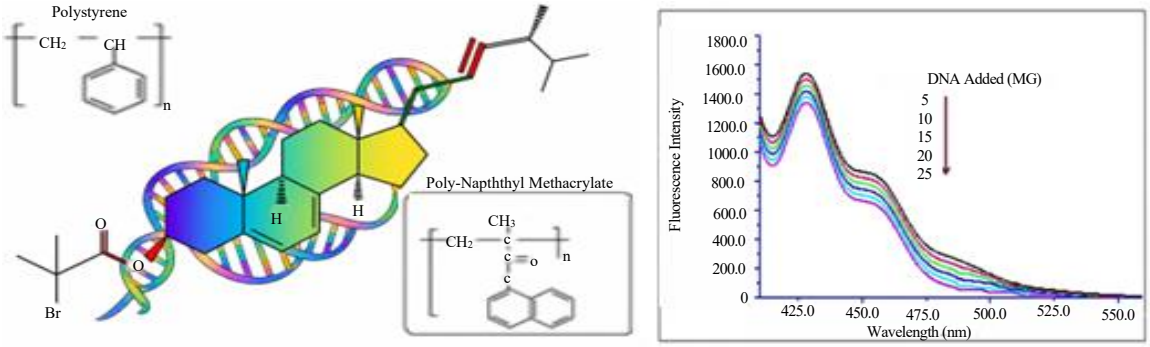

***Author for Correspondence**
N. Haridharan
E-mail: drnharidharan@veltech.edu.in

[1]Research Scholar, Department of Chemistry, Vel Tech Rangarajan Dr. Sagunthala R&D Institute of Science and Technology, Chennai, Tamil Nadu, India
[2]Professor, Department of Chemistry, Vel Tech Rangarajan Dr. Sagunthala R&D Institute of Science and Technology, Chennai, Tamil Nadu, India

Received Date: July 14, 2026
Accepted Date: July 30, 2026
Published Date: August 12, 2026

Citation: S. Prakash, N. Haridharan. Studies on the Self-Assembly of Steroids and DNA Mediated by Naphthalene-Based Amphiphilic Block Copolymer. Journal of Polymer & Composites. 2026; 14(5): 183–196p.

Keywords: Living radical polymerization, ATRP, fluorescent polymers, DNA, amphiphilic block copolymer, steroid

INTRODUCTION

Most of the steroid hormones can regulate moulting, metamorphosis, reproduction and diapause in the human body [1]. It might be investigated that similar roles can be performed in many other invertebrates and still under research. Steroid hormones regulate cellular responses through their interaction with specific receptor proteins localized in the cytoplasm of target cells. Upon binding, the hormone–receptor complex undergoes activation and translocates into the nucleus, where it recognizes and binds to specific DNA sequences or chromatin-associated proteins. This interaction regulates gene expression by enhancing the transcription of target genes [2]. In addition to their biological activity, steroid derivatives exhibit a strong tendency to self-associate in aqueous environments, primarily because of their ability to organize into liquid crystalline phases [3, 4]. An exceptionally interesting case concerns ergosterol esters and their application in gene therapy delivery systems. Functionalization of amphiphilic block copolymers with ergosterol affords mesogenically modified water-soluble polymers, which represent a novel class of materials with unique self-assembly characteristics and can be synthesized through appropriate chemical modification of water-soluble polymer backbones. If the steroid is bound to macromolecules with specific water-soluble groups that can influence the interaction and self-assembly with DNA.

Synthetic polymers incorporating biologically active functional groups have attracted significant focus because of their feasible applications in biomedical science [5]. Among these, glycopolymers containing pendant carbohydrate moieties are of particular interest due to their involvement in essential biological events, including cell recognition, bacterial and viral adhesion, and fertilization [6–8]. Traditionally, these materials have been prepared using conventional free radical polymerization (CFRP), a versatile technique that is generally compatible with a vast range of functional groups and may be carried out in aqueous media [9]. However, CFRP often produces polymers with broad molecular weight distributions and high molecular weights, limiting precise control over polymer architecture [10].

Controlled/living radical polymerization methods were especially developed to address these kinds of limitations. For example, Fukuda and co-workers synthesized well-defined artificial glycolipids through nitroxide-mediated living radical polymerization and subsequently prepared a sequence of glycopolymers using ATRP [11]. Since its introduction in 1995, ATRP has become one of the most widely adopted [12] controlled/living radical polymerization (CLRP) techniques due to its capability to synthesize well-defined polymers with predictable molecular weights and low dispersity. The outstanding capability of ATRP to precisely regulate polymer architecture, molecular weight, and end-group functionality has established it as one of the most versatile controlled/living radical polymerization techniques [13]. Furthermore, the method is strictly compatible with a broad range of functional groups present in initiators [14], monomers, and solvents, making it highly versatile in the synthesis of functional polymers. The use of functional initiators permits the controlled introduction of specific end-group functionalities into polymer chains, provided that these functionalities remain stable throughout the polymerization process [15].

An important challenge in metal-catalyzed living radical polymerization is to simultaneously accelerate the polymerization rate and maintain excellent control over molecular weight and dispersity [16, 17]. Achieving controlled polymerization under ambient conditions, particularly at room temperature, requires the careful selection of both the alkyl halide initiator and the catalytic system. In this regard, Haddleton and co-workers developed a copper(I) Schiff base catalyst that enabled the controlled radical polymerization of acrylate monomers and facilitated the synthesis of polymers possessing diverse functional end groups [18]. In addition, naturally occurring alcohols, especially simple carbohydrates, represent attractive precursors for ATRP initiators because they are inexpensive, readily available, and biologically relevant. Such carbohydrate-derived initiators provide access to

functional polymers with potential applications in biological systems, including processes related to fertilization and molecular recognition [19].

The synthesis and characterization of fluorescent polymers have attracted considerable research interest in recent years [20, 21]. Polymers incorporating fluorescent moieties have found widespread applications in bioimaging, the investigation of polymer physicochemical properties, environmental sensing, electroluminescent devices, plastic colorants, and chemical sensing systems for the detection of pathogens and toxins [22]. A fluorescent moiety could specifically bind to human albumin, which results in the quenching of fluorescence. Wiegand et al. recently reported the development of a novel fluorescent cholesterol derivative, 6-dansylcholesterol, in which a dansyl fluorophore is covalently attached to the steroid nucleus at sixth carbon atom [23]. The dansyl chromophore is widely employed as a fluorescent label for proteins, peptides and lipids because of its strong environmental and societal sensitivity, high intense fluorescence, and sufficiently long excited-state lifetime [24]. Fluorescent cholesterol analogues have become valuable tools for investigating cholesterol distribution and dynamics in biological membranes owing to their high sensitivity, excellent temporal resolution, and ability to provide multiple fluorescence-based parameters [25]. Motivated by these advantages, the present work focuses on the synthesis of steroid end-functionalized amphiphilic polymers containing fluorescent moieties [26]. The synthesized polymers were subsequently characterized, and their self-assembly behavior as well as their interactions with DNA were systematically investigated [27].

EXPERIMENTAL SECTION

The experimental procedures, including the selection of raw materials, synthesis protocols, curing conditions, and characterization methods, are outlined in this section. All measurements were performed under controlled laboratory conditions using calibrated instruments.

Materials

Styrene, methyl methacrylate (MMA), dimethylaminoethyl methacrylate (DMAEMA), tert-butyl acrylate (t-BA) and tert-butyl methacrylate (t-BMA), were obtained from Aldrich. Prior to polymerization, all monomers were purified by passing them through a neutral alumina column (Al_2O_3) to remove inhibitor residues. Copper(I) bromide (CuBr), 2-Bromoisobutyryl bromide, trifluoroacetic acid (TFA), copper(I) chloride (CuCl), ergosterol, anisole, and N,N,N′,N″,N″-pentamethyldiethylenetriamine (PMDETA) were the initiators and ligands, also procured from Aldrich and used without any additional purification. Naphthyl methacrylate (NMA) was synthesized following the reported literature procedure. Triethylamine and tetrahydrofuran (THF) were purified by distillation before using in the synthesis.

Methods

The NMR spectra were acquired on a Bruker Avance 400 spectrometer (400 MHz for ^1H) in $CDCl_3$ or D_2O, as appropriate, at room temperature. High-resolution scanning electron microscopy (HR-SEM) images were obtained using an FEI Quanta 200 scanning electron microscope operated at an accelerating voltage of 30 kV. The AFM was recorded using the Digital Instruments Dimension 3100 AFM system and images were obtained in the contact mode. Fourier-transform infrared (FT-IR) spectra were recorded using a Nicolet 6700 FT-IR spectrometer. UV–Vis absorption spectra were obtained on a JASCO V-530 UV–Vis spectrophotometer. Mass spectra were acquired using a JEOL GCmate II GC–MS spectrometer. Fourier-transform infrared (FT-IR) spectra were recorded using a Nicolet 6700 FT-IR spectrometer. UV–Vis absorption spectra were obtained on a JASCO V-530 UV–Vis spectrophotometer. Mass spectra were acquired using a JEOL GCmate II GC–MS spectrometer. Molecular weight and dispersity were determined by gel permeation chromatography (GPC) using a WATERS GPC system equipped with a refractive index detector (Waters 2410) and a series of columns with pore sizes of 10^3, 10^4, and 10^5 Å (average particle size: 5 μm). Polystyrene (PS) standards were used for calibration, with tetrahydrofuran (THF) as the eluent at a flow rate of 1.0 mL min^{-1}. Data acquisition and analysis were performed using Empower® software (Waters). Fluorescence spectra were recorded on a HITACHI F-4500 spectrofluorometer with an excitation wavelength of 390 nm and

an emission wavelength of 430 nm. The scan speed was maintained at 2400 nm min^{-1}, and both the excitation and emission slit widths were set to 5.0 nm. For fluorescence measurements, polymer solutions were prepared by dissolving an appropriate amount of polymer in 10 mL of THF or water, as appropriate, to obtain a final concentration of 1.0×10^{-5} mol L^{-1}.

Synthesis of Ergosterol Based Initiator

To a three-neck round-bottom flask equipped with a magnetic stirrer, triethylamine (0.22 mol) and ergosterol (0.20 mol) were dissolved in 400 mL of THF. 2-bromoisobutyryl bromide (0.22 mol) was added slowly using a micro-syringe under continuous stirring. A typical orange precipitate of Triethylammonium bromide was formed during the addition, indicated the progress of esterification reaction. To ensure complete conversion, the reaction mixture was stirred continuously for 6h. The precipitated triethylammonium bromide was filtered and using a rotary evaporator the residual solvent was evaporated under reduced pressure. Column chromatography was used to purify the crude products, and the purified initiator was characterized by ^{1}H NMR, FTIR, and mass spectrometry, following the reported procedure. ^{1}H NMR (400 MHz, $CDCl_3$, d ppm): 1.98 (s, 6H, –C $(CH_3)_2$–), 1.0–1.6 (m, CH_2 protons of rigid chain), ^{13}C NMR (100 MHz, $CDCl_3$, d ppm): 29.9 (aliphatic CH_2 carbon), 19.4, 20.7, 24.6 (aliphatic CH_3 carbons), 30.2 (aliphatic $(CH_3)_2$ carbon), 27.7, 27.3, 44.0, 56.5 (CH_2 cyclopentane carbons), 23.2, 28.4, 33.6, 36.1, 37.4, 38.5 (CH_2 cyclohexane carbons), 50.8, 73.3 (CH cyclohexane carbons), 56.5 (CH cyclopentane carbon), 51.7 (aliphatic quaternary carbon), 121.8 (1-ethylene CH carbon), 140.8 (1-ethylene quaternary carbon), 171.3 (1-carboxyl quaternary carbon) FT-IR (NEAT, cm^{-1}): 1758.6 (C=O, ester from initiator), 892.3, 1611(m) (C–C aliphatic), 2928(s) (overtones aliphatic groups), 2050, 1079(s) (C–O–C). GC–MS (m/z): 535; 516; 525.

Typical Procedure for ATRP

To a flame-dried Schlenk tube containing a magnetic stirring bar, the desired amount of Cu(I) catalyst introduced. The reaction container was subjected to two vacuum–argon purge cycles to establish an inert atmosphere after sealing it with rubber septum. The previously degassed monomer was transferred into the container through a cannula, followed by the addition of the ligand. The mixture was stirred gently until the complete formation of the copper–ligand complex. The ergosterol-derived ATRP initiator was then added, and the polymerization had been carried out at ambient temperature under continuous stirring. The polymerization was terminated by diluting the reaction mixture with tetrahydrofuran (THF) after the desired reaction time. The resulting polymer was isolated after precipitation in a mixture of hexane/methanol, collected, and dried under vacuum. By using neutral alumina column, the residual copper catalyst was successfully removed after passing through it. The purified polymer solution was used to determine the molecular weight and dispersity index (PDI), whereas the polymer structure was also interpreted successfully by ^{1}H NMR spectroscopy.

Characterization of the Polymers by ^{1}HNMR

PMMA (400 MHz, $CDCl_3$, d ppm): (s, 0.93, $–CH_3$), (s, 1.96, $–CH_2$), (s, 3.5, $–OCH_3$); PS (400 MHz, $CDCl_3$, d ppm): (m, 6.3–7.0, aromatic protons), (s, 0.7–1.78, aliphatic CH, CH_2 protons); P(S-b-t-BA) (400 MHz, $CDCl_3$, d ppm): (m, 6.5–7.0 aromatic protons), (s, 1.38 O–(C–$(CH_3)_3$), (m, 1.8–2.2 CH, CH_2 protons); PMMA-b-P(DMAEMA-co-NMA) (400 MHz, $CDCl_3$, d ppm): (m, 7.3–7.6 napthyl protons), (t, 4.04 O(CH_2)), (t, 2.55 N–(OCH_2)), (s, 2.27 N–O(CH_3)), (s, 3.58 O(CH_3)), (m, 1.8–1.9 C–(CH_2); PS-b-P(t-BA-co-NMA) (400 MHz, $CDCl_3$, d ppm): (m, 6.5–7.0 styryl protons), (s, 1.38 O $(CH_3)_3$), (m, 1.8–2.2 C (CH_2)), (m, 7.3–7.6 napthyl protons); P(MMA-b-NMA) (400 MHz, $CDCl_3$, d ppm): (m, 7.3–7.6 napthyl protons), (s, 3.53 O (CH_3)), (m, 1.7–1.9 C–(CH_2), (m, 0.7–1.0 C–(CH_3)); P(S-b-NMA) (400 MHz, $CDCl_3$, d ppm): (m 7.3–7.6 napthyl protons), (m 6.3–7.0 styryl protons), (m, 0.7–1.78 aliphatic CH, CH_2 protons); P(MMA-b-DMAEMA) (400 MHz, $CDCl_3$, d ppm): (s, 3.53 O (CH_3)), (t, 3.99 O (CH_2), (t, 2.51 N–(OCH_2), (s, 2.22 N–O (CH_3)),), (m, 1.7–1.8 C–(CH_2), (m, 0.7–1.0 C–(CH_3)); P(S-b-DMAEMA) (400 MHz, $CDCl_3$, d ppm): (m, 6.3–7.0 aromatic protons), (t, 3.99 O (CH_2), (t, 2.5 N–(OCH_2), (s, 2.24 N–O (CH_3), (m, 1.75–1.8 C–(CH_2),), (m, 0.7–0.98) C (CH_3).

Synthesis of Block Copolymers via ATRP

The poly (methyl methacrylate) (PMMA) or poly(styrene) (PS) macroinitiator was transferred to the

reaction container, accompanied by the addition of a mixed solvent system containing acetone and anisole in a 6:4 (v/v) ratio. The reaction mixture was stirred thoroughly and deoxygenated by purging with nitrogen. After complete degassing, the catalyst system comprising CuX and the ligands PMDETA/HMTETA was introduced into the flask. The desired monomer was then added, and the reaction mixture was subjected to a second nitrogen purge to ensure an oxygen-free environment. Polymerization was carried out at 90°C for the predetermined reaction time. Upon completion, the crude polymer solution was passed through a neutral alumina (Al_2O_3) column to remove the copper catalyst and subsequently precipitated into an excess methanol/water mixture to isolate the purified block copolymer. The obtained polymers were suitably characterized by ^{1}H NMR, ^{13}C NMR, gel permeation chromatography (GPC), atomic force microscopy (AFM), Fourier-transform infrared (FTIR) spectroscopy, scanning electron microscopy (SEM), and thermogravimetric analysis (TGA).

RESULTS AND DISCUSSION

To investigate the interactions between amphiphilic block copolymers and biomolecules, metal-catalyzed living radical polymerization (LRP) of monomers, such as methyl methacrylate (MMA) and styrene [28], was carried out in solution at both ambient and elevated temperatures. For this purpose, an atom transfers radical polymerization (ATRP) initiator (R-X) featuring an ergosterol end-group was synthesized. The structure of the synthesized initiator was comprehensively confirmed via ^{1}H NMR as shown in Figures 1 and 2.

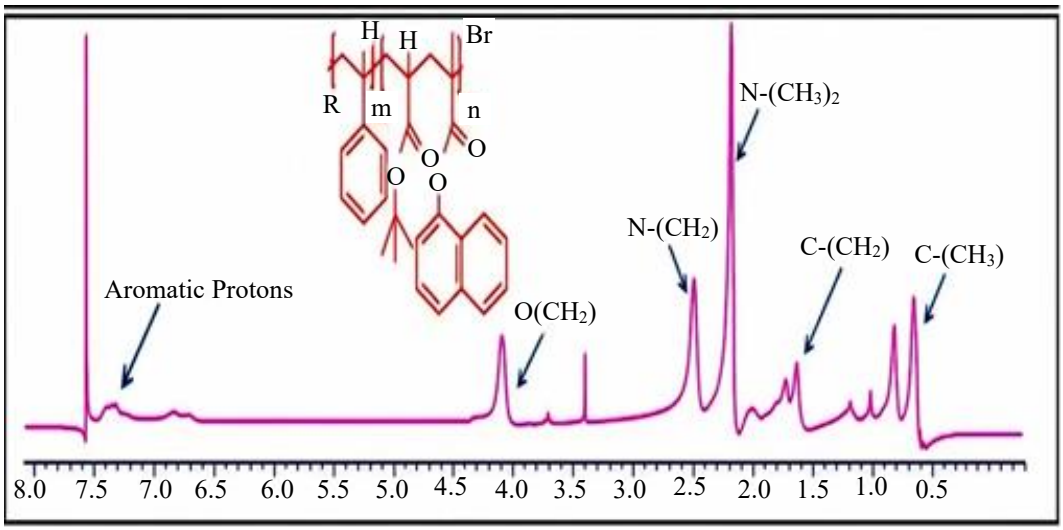

Figure 1. ^{1}H-NMR of P(MMA)-b-P(DMAEMA-co-NMA)].

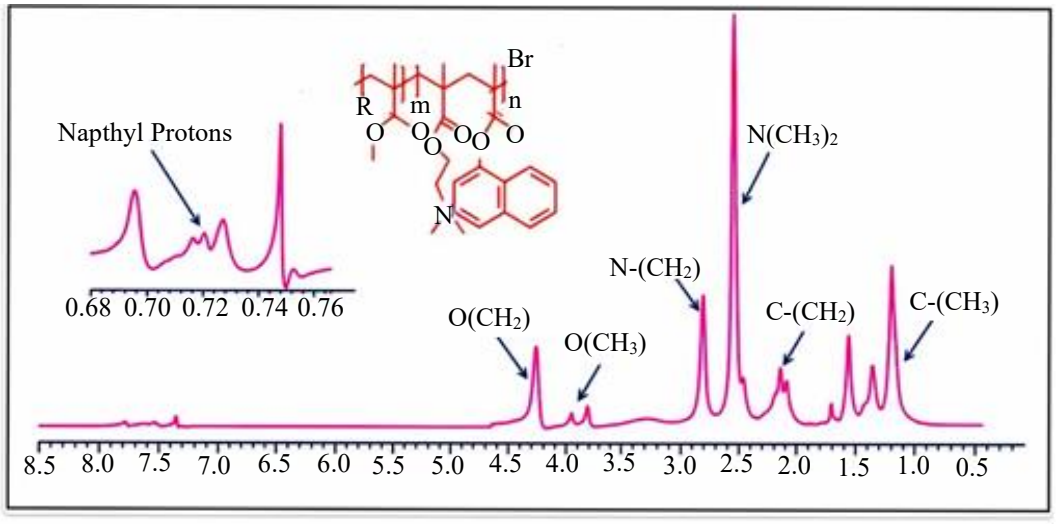

Figure 2. ^{1}H-NMR of [PS-b-P(t-BA-co-NMA)].

The details associated with the polymerization of MMA, styrene and the various combinations of block copolymers using water soluble monomers like N, N-dimethylaminoethyl methacrylate (DMAEMA) and fluorescent monomers – such as 2-napthyl methacrylate (NMA) utilizing Cu(I)Br/PMDETA catalyst system – are detailed in Table 1. In the beginning, the optimum conditions for ATRP of MMA were subjected to take place in both solution and bulk (anisole 50% v/v) and the results are shown in Table 1. From the obtained results, it was clear that the polymerization in bulk was faster in comparison to that in solution and that Cu (I) Br initiated polymerization was faster than that initiated by Cu(I)Cl. This has been reported before by a number of researchers, including us [29]. Although polymerization in solution (50% v/v) is slower, it is better controlled and hence solution polymerization conditions (CuBr: PMDETA: initiator = 1:1:1 and 50% v/v anisole) were used for further studies.

The experimental data clearly show that both monomer conversion and molecular weight increase over time. This trend aligns perfectly with typical living radical polymerization kinetics. Interestingly, the number-average molecular weight (Mn) measured by gel permeation chromatography (GPC) was lower than the theoretical values calculated from monomer conversion. This discrepancy likely stems from the universal calibration method, which utilizes narrow polystyrene (PS) standards instead of polymethyl methacrylate (PMMA) standards. To achieve optimal control over a polymerization process, the initiation rate must exceed the propagation rate. In this study, the close agreement between the experimental Mn (GPC) and theoretical Mn (theoretically calculated) values during solution polymerization indicates that this specific method offers superior control over the reaction.

The optimal studies of the ATRP of styrene monomer was also performed in solution [diphenyl ether (DPE) 50% v/v] and from the it is also clear that the polymerization in solution is faster (and less controlled), if the concentration of the monomer is higher and if CuBr is used instead of CuCl. Although polymerization is slower at 60°C, it is more controlled (Table 1, entries 4 and 5). In order to retain control, without much loss in the rate of polymer production, the solution polymerization of styrene was carried out at 90°C in 50% (v/v) DPE [30]. The Mn (GPC) and PDI values were plotted against monomer conversion. It is clear that Mn (GPC) is greater than Mn (expected) suggesting that some of the initiator molecules could be lost by bimolecular termination, in the earlier stages of the reaction [31]. It can also be seen that the PDI decreases with polymerization time, which is often due to the generation of greater concentration of Cu (II), the persistent radical, with time. The Mn versus (%) conversion curve indicates a very poor initial control over polymerization. Thus, in the case of styrene polymerization, bimolecular termination of initiator radicals is higher than that in the case of MMA [32]. This could be due to the intrinsic slower polymerization kinetics of styrene in comparison with MMA.

The block copolymers, P(S-b-NMA)-Br, P(S-b-t-BA)-Br, PS-b-P(t-BA-co-NMA)-Br, P(S-b-DMAEMA)-Br, P(MMA-b-DMAEMA)-Br and PMMA-b-P(DMAEMA-co-NMA)-Br were synthesized successfully by ATRP yielding well organized di-block and multi-block copolymers with PDI value (Mw/Mn) < 1.1 and also confirmed by means of NMR spectroscopy as shown in the ^{1}H – NMR readings.

The characteristics of the block copolymers obtained from GPC are reported in detail in Table 1. In general, the Polydispersity Index was observed to be increased upon polymerizing a second and third monomer.

Table 1. GPC characteristics of block copolymers.

S. N.	First block	Block copolymer	Mn (GPC)	PDI
1	PS-Br(135) (a) Mn = 14000; PDI = 1.33	P(S135-b-t-BA240)-Br(b)	45000	*1.45*
2	PS-Br(135) (a)	P(S135-b-NMA38)-Br(c)	22000	*1.46*

	Mn = 14000; PDI = 1.33			
3	PS-Br(135) (a) Mn = 14000; PDI = 1.33	PS135-b-P(t-BA290-co-NMA30)-Br(d)	57400	*1.5*
4	PMMA-Br(110) (e) Mn = 11000; PDI = 1.38	PMMA110-b-P(DMAEMA56-co-NMA10)-Br(f)	22000	*1.49*
5	PMMA-Br(110) (e) Mn = 11000; PDI = 1.38	P(MMA110-b-DMAEMA16)-Br (g)	13600	*1.52*
6	PMMA-Br(110) (e) Mn = 11000; PDI = 1.38	P(MMA110-b-NMA29)-Br(h)	17200	*1.47*

(a) [initiator]: [CuBr]: [PMDETA] = 1:1:1 in DPE at 90°C;
(b) [PS-Br]: [CuBr]: [PMDETA] = 1:1:1 in anisole/acetone at 90°C.
(c) [PS-Br]: [CuBr]: [PMDETA] = 1:1:1 in anisole at 90°C.
(d) [PS-Br]: [CuBr]: [PMDETA] = 1:1:1 in anisole/acetone at 90°C copolymer composition calculated from ^{1}H NMR.
(e) [initiator]: [CuBr]: [PMDETA] = 1:1:1 in anisole at 30°C.
(f) [PMMA – Br]: [CuBr]: [PMDETA] = 1:1:1 in THF/acetone at 90°C copolymer composition calculated from ^{1}H NMR.
(g) [PMMA-Br]: [CuBr]: [PMDETA] = 1:1:1 in THF at 30°C.
(h) [PMMA-Br]: [CuBr]: [PMDETA] = 1:1:1 in anisole at 90°C.

The block copolymer of P(MMA-b-DMAEMA) was also successfully synthesized, at desired temperature [33], with CuBr/HMTETA catalyst. The block polymerization was also confirmed by means of TGA, which show necessary decompositions at particular temperatures highlighted in the (Figures 3 & 4). Thermogravimetric analysis (TGA) of the block copolymers reveals characteristic two-stage thermal decompositions. For P(S-*b*-*t*-BA), the first degradation occurs around 240°C due to the *t*-BA block, followed by a broad transition from 320°C to 460°C corresponding to the PS block. In contrast, both P(S-*b*-DMAEMA) and P(MMA-*b*-DMAEMA) exhibit initial decomposition around 280°C, attributed to the DMAEMA block. Their second degradation stages occur as broad transitions from 330°C to 460°C for the PS block and 350°C to 460°C for the PMMA block, respectively.

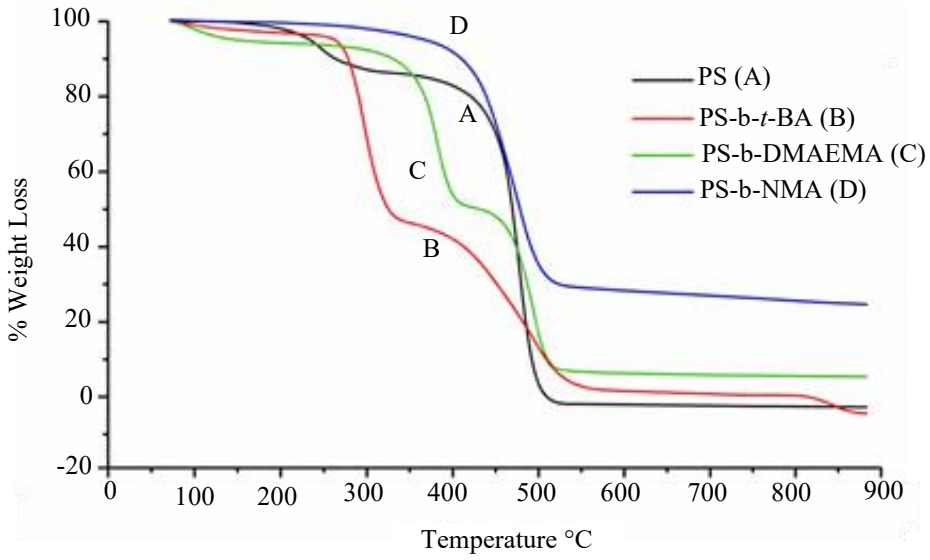

Figure 3. Thermal measurements for polystyrene and its related block copolymers.

The polymers with a block of poly (t-butyl acrylate) and poly (t-butyl methacrylate) were hydrolyzed to poly (acrylic acid) and poly (methacrylic acid) by using trifluoroacetic acid as the catalyst in dichloromethane (DCM) at room temperature [34, 35] and the polymers were characterized using FT-IR. The peak at 1143 cm^{-1} is assigned to the t-butyl group of the block copolymer, whereas in the case

of the block copolymer P(S-b-AA), the disappearance of the peak at 1143 cm^{-1} confirms the hydrolysis of t-butyl group and the appearance of a broad peak around 3500 cm^{-1} confirms the formation of the carboxylic acid groups.

The fluorescence emission spectra of the polymer solutions are shown in Figure 5**.** The fluorescence emission spectra were recorded with excitation at 390 nm. The emission spectrum is red shifted and is seen around 400 to 500 nm [36]. The emission spectrum of NMA shows three distinct and identifiable emission peaks at 405 nm, 430 nm and 455 nm. These can be attributed to the relaxation from the first excited electronic state to higher vibrational levels of the ground electronic state.

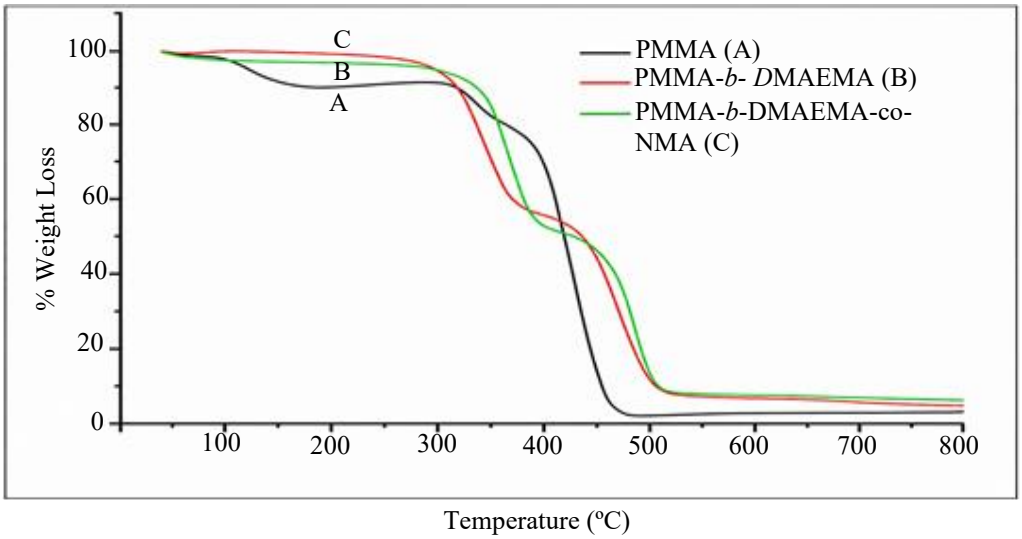

Figure 4. Thermal measurements for P(MMA) and its block copolymers.

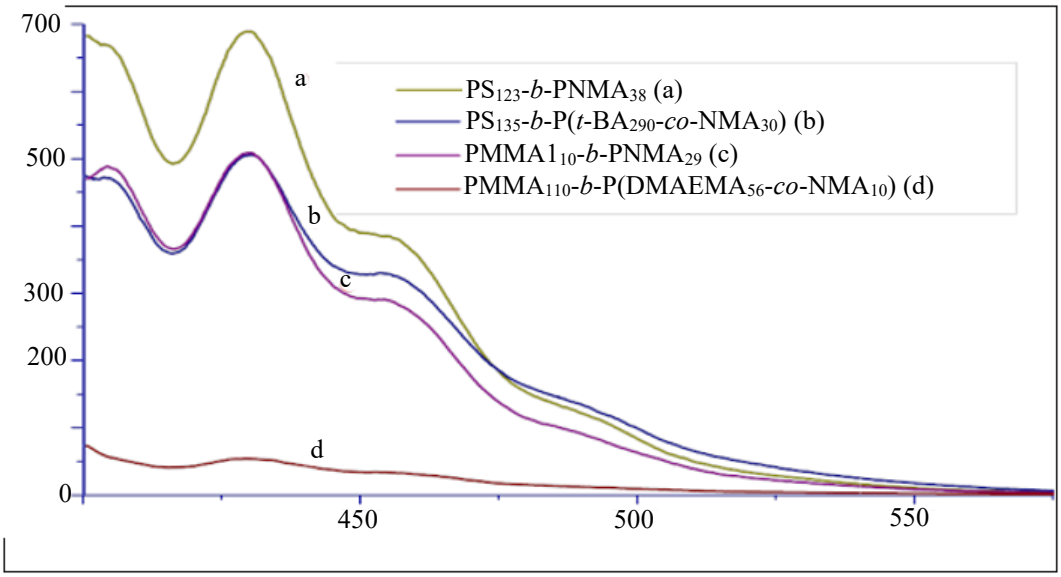

Figure 5. Fluorescence emission spectra of block copolymers in THF; 10–5 moles/L (excited at 390 nm).

It can be seen that all the block copolymers based on NMA show emissions, like NMA, as shown in Figure 5, thus confirming the presence of NMA. Further, the emission pattern from the block copolymer containing NMA is not different from that of pure NMA suggesting that the fluorescence emission fine structure is not altered due to polymerization or due to polymer conformations in solution. However, PMMA-b-P(DMAEMA-co-NMA) shows relatively lesser emission at the expected wavelength in part due to lower composition and concentration of the NMA moiety and probably due to poor interaction

with THF [37]. The hydrolysis of the PMMA component of the above block copolymer results in PMMA-b-P(DMAEMA-co-NMA), which is water soluble due to the presence of methacrylic acid groups. The fluorescence emission spectrum of this block copolymer shows that its interaction with water is better as can be seen by the appearance of the characteristic emission spectrum of NMA, as shown in Figure 5.

The self-assembly of this block copolymer with DNA was studied using fluorescence quenching measurements [38]. DNA was chosen for binding studies because the inclusion of DNA in to a block copolymer can lead to protect from degrading enzymes and affords an improved biological effect attributed to sustained and localized release [39] and also for non-viral gene delivery [40] along with water soluble polymers. The polymer PMAA-b-P(DMAEMA-co-NMA) was chosen for binding studies with the DNA as it is a fluorescent zwitter-ionic diblock copolymer and its properties can be tuned with change of pH in the aqueous medium. An aqueous solution of the polymer was added to a known amount of DNA, and the fluorescence emission was recorded with excitation at 390 nm, as shown in Figure 6.

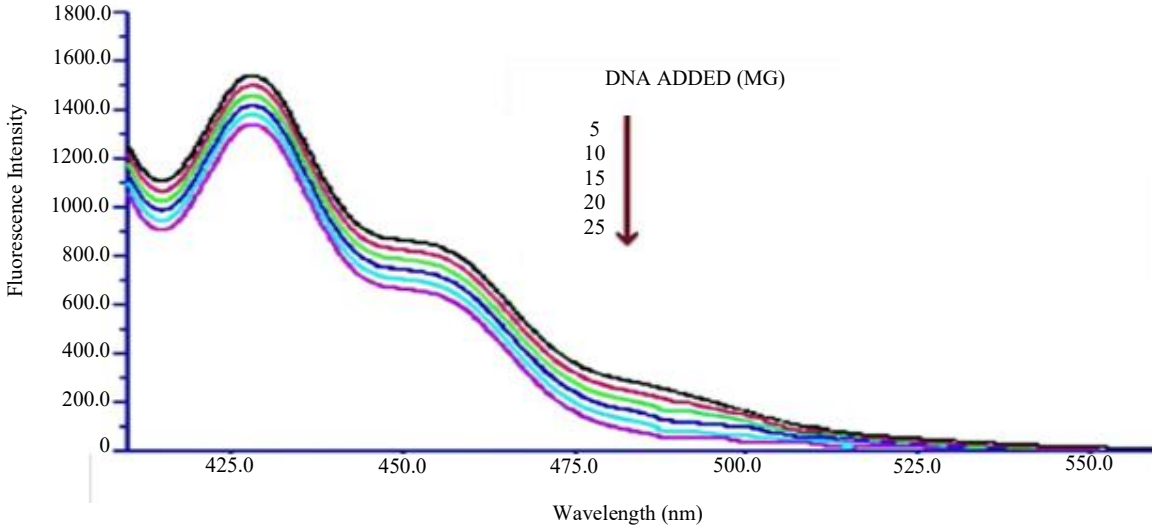

Figure 6. Fluorescence emission spectrum (quenching) of block copolymer P (MAA)-b-(DMAEMA-co NMA) in aqueous medium (excited at 390 nm), with the addition of DNA (horse herring sperm).

The self-assembly of this block copolymer with DNA was investigated by fluorescence quenching measurements. Upon the gradual addition of DNA, a progressive decrease in the fluorescence intensity of PMAA-b-P(DMAEMA-co-NMA) was observed without the appearance of new emission bands, indicating efficient fluorescence quenching [41] resulting from polymer–DNA complex formation. The fluorescence quenching is attributed to the close association of the polymer chains with DNA, which modifies the local microenvironment surrounding the naphthalene fluorophore and promotes non-radiative relaxation of the excited state.

Electrostatic attraction between the protonated dimethylamino groups of the DMAEMA segments and the negatively charged phosphate backbone of DNA serves as the primary driving force for complex formation. Simultaneously, the amphiphilic nature of the block copolymer promotes hydrophobic association of the ergosterol and naphthalene moieties, resulting in the formation of compact self-assembled nanostructures that stabilize the polymer–DNA complexes. The observed concentration-dependent fluorescence quenching, therefore, provides strong evidence for efficient polymer–DNA interaction and supports the proposed self-assembly mechanism [42].

Scanning electron microscopy (SEM) and atomic force microscopy (AFM) were employed to analyze the surface morphology of the block copolymers (Figures 7–8). SEM analysis reveals distinct self-

assembled morphologies for the copolymers depending on their block composition and casting solvent. When spin-coated from a DMF solution, P(S-*b*-*t*-BA) displays a unique "jasmine bud-like" architecture, which can be attributed to the specific aggregation behavior of the *t*-butyl blocks (Figure 7). In contrast, spin-coating the PS-*b*-P(*t*-BA-*co*-NMA) block copolymer from THF yields a highly ordered, honeycomb-like microarray characterized by hexagonal close packing (Figure 8). Interestingly, the introduction of the naphthyl group drives phase separation, prompting the formation of spherical domains with diameters ranging from 0.3 to 2.5 μm, though some irregularities in domain shape and packing layout persist.

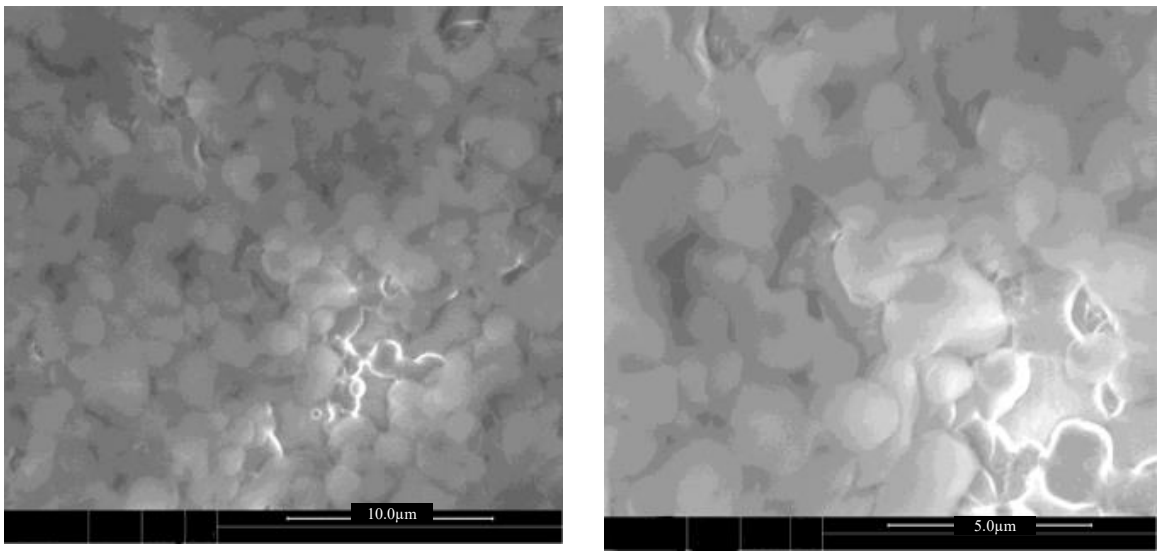

Figure 7. SEM micrographs of the block copolymer P(MMA)-b-P(DMAEMA-co-NMA)] spin-coated onto a glass slide from a 10 mg/mL DMF solution at varying magnifications.

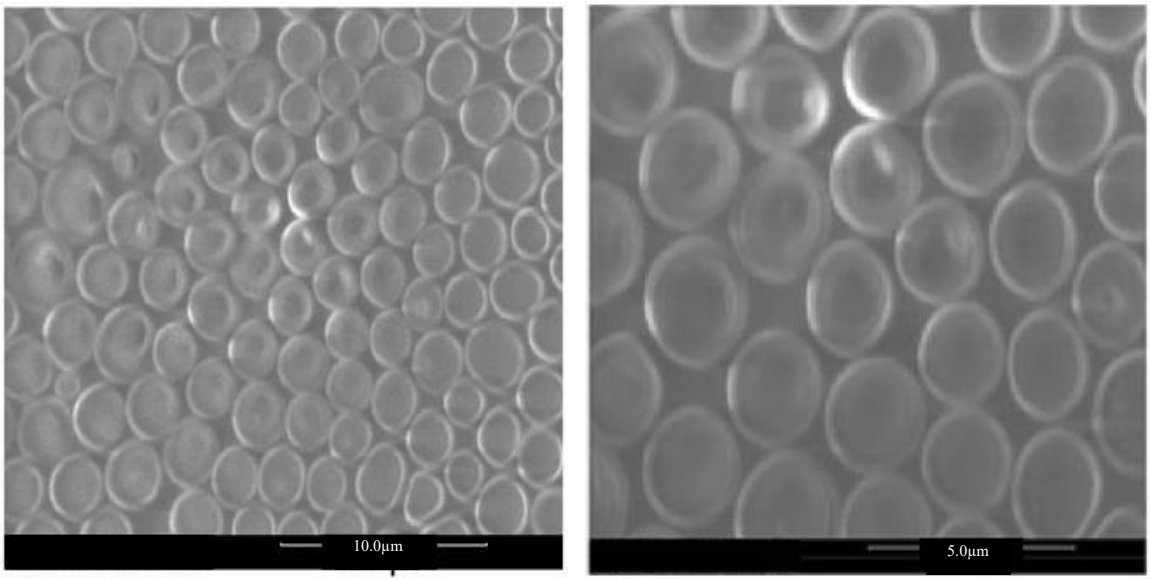

Figure 8. SEM images at different magnifications of spin-coated [PS-b-P(t-BA-co-NMA)] (10 mg/mL in THF) on glass slides.

The SEM images of the block copolymer Pt-BMA-b-P(NMA-co-DMAEMA), spin coated from THF produces flower and foldable paper, like morphologies, which may be attributed to the formation of micelles of the amphiphilic block copolymer (37, 38).

The zwitter ionic block copolymer can be well tuned by change of pH, which can be monitored by

SEM analysis (Figures 7 & 8).

The AFM image of the block copolymer P(MMA)-b-P(DMAEMA-co-NMA)] and [PS-b-P(t-BA-co-NMA)] dip coated in DMF produces different morphology. In the case of P(S-b-t-BA), irregular hollow shape arrangement of smaller dimension 0.2 to 1.0 µm and larger dimensions 0.2 to 1.4 µm were seen whereas in the case of the same polymer after hydrolysis, ring – like morphology – is seen (as shown in Figure 9.

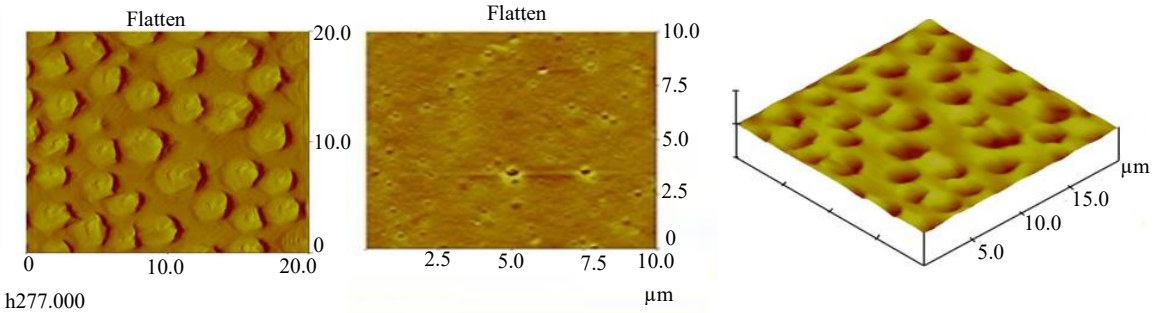

Figure 9. AFM image of block copolymer PS-b-t-BA (left) and PS-b-AA (right) in DMF; concentration of 10 mg/ml (dip coated on the microscopic glass plate).

CONCLUSIONS

A bioactive ergosterol-derived atom transfer radical polymerization (ATRP) initiator was synthesized successfully and its structure was confirmed using appropriate spectroscopic techniques. The initiator was effectively incorporated for the preparation of a series of novel synthetic and amphiphilic block copolymers incorporating fluorescent naphthyl methacrylate units through controlled ATRP under both ambient and elevated temperature conditions. The resulting copolymers exhibited comparatively narrow molecular weight distributions ($M_w/M_n < 1.5$) predictable molecular weights and demonstrating the controlled nature of the polymerization process. Polymerization kinetics and molecular weight analyses indicated that the steric characteristics of the ergosterol-based initiator influenced the propagation rate, leading to comparatively slower but well-controlled polymer growth. Nevertheless, the initiator proved to be highly suitable for controlled polymerization, particularly under mild reaction conditions. The synthesized block copolymers were comprehensively characterized to evaluate their structural, thermal, and fluorescence properties. Their surface morphology was further examined using scanning electron microscopy (SEM) and atomic force microscopy (AFM), revealing a variety of self-organized nanostructures, including jasmine bud-like, folded sheet-like, and honeycomb-like morphologies, depending on the polymer composition. The self-assembly behavior of these amphiphilic block copolymers in aqueous media is currently being investigated in greater detail through physicochemical studies. Among the synthesized materials, PMMA-b-P(DMAEMA-co-NMA) displayed strong fluorescence emission in aqueous solution, whereas a significantly weaker emission was observed in tetrahydrofuran (THF), indicating pronounced solvent-dependent photophysical behavior arising from specific polymer–solvent interactions. Following hydrolysis, this block copolymer exhibited effective interaction with DNA, as evidenced by a progressive decrease in fluorescence intensity upon increasing DNA concentration. The observed fluorescence quenching confirms the formation of polymer–DNA complexes and provides clear evidence for the self-assembly of the steroid-functionalized amphiphilic block copolymers in aqueous environments.

Declarations

We declare that I have no known competing financial interests or personal relationships that could have appeared to influence the work reported in this paper.

Author Contributions

- *S. Prakash* – Experimental work, resources, writing – original draft, review, & editing.

- *N. Haridharan* – Experimental work, characterization, investigation, conceptualization, methodology, supervision, validation, visualization, formal analysis, writing – original draft, review, & editing.

Funding

Not applicable.

Acknowledgment

The authors thank IIT Madras for instrumental analysis.

REFERENCES

1. Dinan L, Lafont R. Effects and applications of arthropod steroid hormones (ecdysteroids) in mammals. J Endocrinol. 2006;191(1):1–8. doi: 10.1677/joe.1.06900.
2. Spelsberg T, Goldberger A, Hora J, Horton M, Littlefield B. Characterization of the nuclear binding sites (acceptor sites) for a steroid receptor. In: Roy AK, Clark JH, editors. Gene Regulation by Steroid Hormones III. New York, NY: Springer New York; 1987. p. 111–136. doi: 10.1007/978-1-4612-4686-2_8.
3. Galanov EK, Kostyuk GK, Mukhina MV, Kostrov ID, Mel'nik RI. Study of phase transformations in various cholesteric liquid crystals. J Struct Chem. 1977;17(4):599–603. doi: 10.1007/BF00753446.
4. Umamaheshwari RB, Jain NK. Receptor-mediated targeting of lipobeads bearing acetohydroxamic acid for eradication of Helicobacter pylori. J Control Release. 2004;99(1):27–40. doi: 10.1016/j.jconrel.2004.06.006.
5. Satchanska G, Davidova S, Petrov PD. Natural and synthetic polymers for biomedical and environmental applications. Polymers. 2024;16(8):1159. doi: 10.3390/polym16081159.
6. Glycosylation: Mechanisms, biological functions and clinical implications. Signal Transduct Target https://www.nature.com/articles/s41392-024-01886-1.
7. Various biological functions of carbohydrate chains learned from glycosyltransferase-deficient mice. https://pmc.ncbi.nlm.nih.gov/articles/PMC7445053/.
8. Reading CL. Carbohydrate structure, biological recognition, and immune function. In: Ivatt RJ, editor. The Biology of Glycoproteins. Boston, MA: Springer US; 1984. p. 235–321. doi: 10.1007/978-1-4684-7464-0_5.
9. Liu S. The future of free radical polymerizations. Chem Mater. 2024;36(4):1779–1780. doi: 10.1021/acs.chemmater.4c00312.
10. Gentekos DT, Sifri RJ, Fors BP. Controlling polymer properties through the shape of the molecular-weight distribution. Nat Rev Mater. 2019;4(12):761–774. doi: 10.1038/s41578-019-0138-8.
11. Lamontagne HR, Lessard BH. Nitroxide-mediated polymerization: A versatile tool for the engineering of next generation materials. ACS Appl Polym Mater. 2020;2(12):5327–5344. doi: 10.1021/acsapm.0c00888.
12. Harrisson S, Whitfield R, Anastasaki A, Matyjaszewski K. Atom transfer radical polymerization. Nat Rev Methods Primers. 2025;5(1):2. doi: 10.1038/s43586-024-00370-y.
13. Krys P, Matyjaszewski K. Kinetics of atom transfer radical polymerization. Eur Polym J. 2017;89:482–523. doi: 10.1016/j.eurpolymj.2017.02.034.
14. Kotha S, Gupta NK, Ansari S. One-pot thiol-free synthetic approach to sulfides, and sulfoxides selectively. RSC Adv. 2022;12(39):25154–25162. doi: 10.1039/D2RA04872H.
15. Lee H, Lee Y, Kim N, Park MJ. Polymer chain-end chemistry: Unlocking next-generation functional materials. Prog Polym Sci. 2025;168:102003. doi: 10.1016/j.progpolymsci.2025.102003.
16. Kamigaito M, Ando T, Sawamoto M. Metal-catalyzed living radical polymerization. Chem Rev. 2001;101(12):3689–3746. doi: 10.1021/cr9901182.
17. Sun M, Szczepaniak G, Dadashi-Silab S, Lin TC, Kowalewski T, Matyjaszewski K. Cu-catalyzed atom transfer radical polymerization: The effect of cocatalysts. Macromol Chem Phys. 2023;224(3):2200347. doi: 10.1002/macp.202200347.
18. Liu H, Maugein VA, Haddleton DM. Radical polymerisation and thiol-ene post-polymerisation functionalisation of terpenoid acrylates in conventional and renewably sourced organic solvents. Polym Chem. 2024;15(28):2862–2872. doi: 10.1039/D4PY00340C.

19. Luo X. Biomass-derived carbon dots for the initiation of conventional radical and ATRP-based photopolymerization processes. Nat Protoc. 2025;20(12):3695–3721. doi: 10.1038/s41596-025-01210-3.
20. Zhong H, Zhao B, Deng J. Synthesis and application of fluorescent polymer micro- and nanoparticles. Small. 2023;19(26):2300961. doi: 10.1002/smll.202300961.
21. Wei S, Zhang Z, Xu Y, Dang D, Zeng R. Covalent installation of fluorophores into polyethylene: Synthesis, characterization, and applications. Macromolecules. 2024;57(8):3595–3603. doi: 10.1021/acs.macromol.4c00381.
22. Xu H, Zhang W, Wang M. Bioinspired fluorescent polymers: Synthesis, processing, and applications. Chin J Chem. 2023;41(4):458–468. doi: 10.1002/cjoc.202200493.
23. Gao S. Albumin tailoring fluorescence and photothermal conversion effect of near-infrared-II fluorophore with aggregation-induced emission characteristics. Nat Commun. 2019;10(1):2206. doi: 10.1038/s41467-019-10056-9.
24. Larson J. The use of dansyl chloride to probe protein structure and dynamics. Int J Mol Sci. 2025;26(2):456. doi: 10.3390/ijms26020456.
25. Milles S. Organization of fluorescent cholesterol analogs in lipid bilayers—Lessons from cyclodextrin extraction. Biochim Biophys Acta Biomembr. 2013;1828(8):1822–1828. doi: 10.1016/j.bbamem.2013.04.002.
26. Biswas S, Rajdev P, Banerjee A, Das A. Mitochondria-targeting nanostructures from enzymatically degradable fluorescent amphiphilic polyesters. Nanoscale. 2025;17(10):5732–5742. doi: 10.1039/D4NR04696J.
27. Li F, Tang J, Geng J, Luo D, Yang D. Polymeric DNA hydrogel: Design, synthesis and applications. Prog Polym Sci. 2019;98:101163. doi: 10.1016/j.progpolymsci.2019.101163.
28. Krishnan A, Roy S, Menon S. Amphiphilic block copolymers: From synthesis including living polymerization methods to applications in drug delivery. Eur Polym J. 2022;172:111224. doi: 10.1016/j.eurpolymj.2022.111224.
29. Chatterjee U, Jewrajka SK, Mandal BM. The amphiphilic block copolymers of 2-(dimethylamino)ethyl methacrylate and methyl methacrylate: synthesis by atom transfer radical polymerization and solution properties. Polymer. 2005;46(24):10699–10708. doi: 10.1016/j.polymer.2005.09.045.
30. Ivchenko PV. Controlled polymerization. Polymers. 2023;15(6):1379. doi: 10.3390/polym15061379.
31. Li S. Synthesis of PAN with adjustable molecular weight and low polydispersity index (PDI) value via reverse atom transfer radical polymerization. Des Monomers Polym. 2019;22:180–186. doi: 10.1080/15685551.2019.1678557.v
32. Vicevic M, Novakovic K, Boodhoo K. Free-radical polymerization of styrene: Kinetic study in a spinning disc reactor (SDR). Front Chem Eng. 2021;3:661498. doi: 10.3389/fceng.2021.661498.
33. Li Z. A controlled synthesis method of alkyl methacrylate block copolymers via living anionic polymerization at ambient temperature. RSC Adv. 2019;9(28):16049–16056. doi: 10.1039/C9RA01577A.
34. Däbritz S. Evaluating polymerization methods and deprotection strategies for making water soluble poly(acrylic acid) with hydrolyzable breaking points. Macromol Chem Phys. 2025. doi: 10.1002/macp.202500080.
35. Rapid and quantitative de-tert-butylation for poly(acrylic acid) block copolymers and influence on relaxation of thermoassociated transient networks. Macromolecules https://pubs.acs.org/doi/10.1021/acs.macromol.8b01440.
36. Penso CM, Castanheira EMS, Paiva MC, Gonçalves LM. Polymer sorting through fluorescence spectra. Bioengineering. 2025;12(7):708. doi: 10.3390/bioengineering12070708.
37. Saraiva GKV. Characterization of PMMA-b-PDMAEMA aggregates in aqueous solutions. Colloid Polym Sci. 2019;297(4):557–569. doi: 10.1007/s00396-019-04482-w.

38. Liu Y, Liu Y, Feng F, Wang W. Self-assembly of block copolymers to prepare advanced materials with hierarchical functional nanostructures. Nanomanufacturing. 2025;5(4):18. doi: 10.3390/nanomanufacturing5040018.
39. DNA-block copolymer conjugates. J Am Chem Soc https://pubs.acs.org/doi/full/10.1021/ja0156845.
40. Khan M. Polymers as efficient non-viral gene delivery vectors: The role of the chemical and physical architecture of macromolecules. Polymers. 2024;16(18):2629. doi: 10.3390/polym16182629.
41. Lietard J, Ameur D, Somoza MM. Sequence-dependent quenching of fluorescein fluorescence on single-stranded and double-stranded DNA. RSC Adv. 2022;12(9):5629–5637. doi: 10.1039/D2RA00534D.
42. Kalinova R, Videv P, Petrova S, Doumanov J, Dimitrov I. Poly(2-(dimethylamino)ethyl methacrylate)-grafted amphiphilic block copolymer micelles co-loaded with quercetin and DNA. Molecules. 2024;29(11):2540. doi: 10.3390/molecules29112540.

